Available online at www.sciencedirect.com
ScienceDirect
Journal of Catalysis 243 (2006) 149–157
JOURNAL OF CATALYSIS
www.elsevier.com/locate/jcat

Model NO_x storage systems: Storage capacity and thermal aging of BaO/θ-Al_2O_3/NiAl(100)

Emrah Ozensoy, Charles H.F. Peden, János Szanyi *

Institute for Interfacial Catalysis, Pacific Northwest National Laboratory, P.O. Box 999, MSIN K8-93, Richland, WA 99352, USA

Received 6 March 2006; revised 26 June 2006; accepted 28 June 2006

Available online 22 August 2006

Abstract

The NO_x storage properties of a BaO/θ-Al_2O_3/NiAl(100) model system, with a BaO coverage of ∼2 monolayer equivalent (MLE), was studied. X-ray photoelectron spectroscopy (XPS) and temperature-programmed desorption (TPD) techniques were used to investigate NO_2 adsorption and reaction on the BaO/θ-Al_2O_3/NiAl(100) surface. These results were compared with those of the θ-Al_2O_3/NiAl(100) support material, a thermally aged BaO/θ-Al_2O_3/NiAl(100) model system, and a realistic BaO (20 wt%)/γ-Al_2O_3 high-surface area counterpart. At $T > 300$ K, adsorbed NO_2 is converted to nitrates on all of the surfaces studied. Nitrates residing on the alumina sites of the model catalyst surfaces are relatively weakly bound and typically desorb within 300–600 K, leading to NO(g) evolution; while nitrates associated with the baria sites are significantly more stable and desorb within 600–850 K, resulting in NO(g) or NO(g) + O_2(g) evolution. NO_x uptake by the baria sites of the BaO/θ-Al_2O_3/NiAl(100) model system was found to be as much as five-fold greater than that of the θ-Al_2O_3/NiAl(100) support material. Thermal aging of a BaO/θ-Al_2O_3/NiAl(100) surface at 1100 K before NO_x uptake experiments brings about a significant (>70%) reduction in the NO_x storage capacity of the model catalyst surface.

Keywords: NO_x storage materials; Al_2O_3; BaO; Pt; NO; NO_2; Nitrate; Nitrite; XPS; TPD

1. Introduction

Due to their outstanding catalytic performance for NO_x reduction under highly oxidizing conditions resulting from diesel engine operation, BaO and transition metal-based NO_x storage/reduction (NSR) catalysts [1–4] have recently become, along with an ammonia selective catalytic reduction (SCR) approach [5], a viable technology solution for controlling NO_x emissions from diesel engine powered vehicles. Diesel engines are typically operated at high air to fuel ratios (A/F = 25/1 [wt/wt]) providing up to a 35% improvement in fuel efficiency with respect to that of gasoline engines in which lower A/F ratios (14.5) are used [5]. It should be noted that conventional (Pd or Pt–Rh)/γ-Al_2O_3-based three-way catalysts (TWC) commonly used in automotive catalysts for NO_x reduction purposes fail under highly oxidizing (lean) conditions, that is, A/F > 18 [1].

The first commercial NSR catalyst was developed in 1994 by Toyota Motor Company [1], where a Pt/BaO/γ-Al_2O_3-based formulation was used. In this catalyst formulation, the Pt component provides NO oxidation and NO_x reduction (redox) capabilities, whereas the primary role of BaO sites is NO_x storage in the form of $Ba(NO_3)_2$. The γ-Al_2O_3 support material enables dispersion of the active sites over a large surface area and may facilitate the reactant transport between the active sites on the catalyst via surface diffusion. NSR catalysts are typically operated in two alternating cycles. In the so-called *storage cycle*, the exhaust gas composition is abundant in O_2 (i.e., lean conditions). Under these conditions, NO(g), which is the major NO_x component in the untreated exhaust gas mixture, is readily oxidized to NO_2 on the Pt sites. Next, NO_2 migrates onto the BaO storage sites via gas-phase adsorption and/or surface diffusion and is eventually stored as $Ba(NO_3)_2$. After saturation of the active Ba-containing phase with nitrates, a *reduction cycle* is started by quickly switching to an exhaust gas-phase composi-

* Corresponding author.
E-mail address: janos.szanyi@pnl.gov (J. Szanyi).

0021-9517/$ – see front matter © 2006 Published by Elsevier Inc.
doi:10.1016/j.jcat.2006.06.028

tion that is abundant in hydrocarbons (HC), CO, and H_2 (i.e., rich conditions). During the reduction cycle, the Ba component releases the stored nitrates in the form of NO_2 and $NO + O_2$, which is subsequently transferred onto the Pt sites to be reduced to N_2, resulting in regeneration of the active BaO storage component [1].

Although numerous studies on high-surface area NSR catalysts have been conducted, as recently discussed in a detailed review by Epling et al. [2], only a limited number of surface science studies [6,7] have been carried out addressing the fundamental chemical and physical phenomena occurring on the NSR catalyst surfaces, which ultimately dictate the reaction mechanisms and catalytic performance of these systems. Therefore, we have recently used a systematic approach to identify some of the key surface science phenomena relevant to the NSR systems by means of well-defined mixed-oxide (baria–alumina)-based model systems. We have used a bottom-up synthetic strategy to prepare a model NO_x storage material. This is achieved by using an ordered θ-Al_2O_3 ultrathin film grown on a NiAl(100) bimetallic alloy substrate mimicking the high-surface area alumina counterpart. The spectroscopic characterization of the alumina support material [8], as well as its interaction with H_2O [8], NO_2 [9], and $H_2O + NO_2$ [10] in the absence of the active Ba-containing phase, have been investigated previously. Next, deposition, oxidation, and growth of the Ba phase on the θ-Al_2O_3/NiAl(100) substrate were studied via different preparation protocols [11,12] to obtain a model NO_x storage system in the form of BaO/θ-Al_2O_3/NiAl(100) [12].

As a continuation of this effort, in the current text we focus on the NO_x storage properties of the BaO/θ-Al_2O_3/NiAl(100) model system on NO_2 adsorption using TPD and XPS techniques. Furthermore, NO_2 uptake of the BaO/θ-Al_2O_3/NiAl-(100) mixed metal-oxide surface, as well as the Ba-free θ-Al_2O_3/NiAl(100) substrate and a realistic high-surface area BaO (20 wt%)/γ-Al_2O_3 NO_x storage material, will be discussed in a comparative fashion. Finally, the thermal aging and deactivation of the NSR systems will be examined. This will be illustrated by NO_2 adsorption and subsequent TPD analysis on a BaO/θ-Al_2O_3/NiAl(100) surface pretreated at high temperatures (1100 K) before NO_x adsorption, in an attempt to simulate some of the long-term thermal aging effects that can occur under regular operational and regeneration temperatures (573–973 K).

2. Experimental

The experimental setup, sample preparation methods and the data acquisition procedures that are used in the current work have been discussed in detail elsewhere [8–12]. In brief, experiments were performed in an ultra-high vacuum (UHV) surface analysis chamber ($P_{base} = 2 \times 10^{-10}$ Torr) equipped with facilities for XPS (PHI-dual anode X-ray source, Omicron EA-125 multichannel electrostatic hemispherical electron energy analyzer), AES (PHI-single pass cylindrical mirror analyzer), a quadruple mass spectrometer (QMS, UTI) for TPD, and a rear-view low energy electron diffraction (LEED) setup (Princeton Research Instruments). θ-Al_2O_3/NiAl(100) surfaces were prepared using the procedure developed by Ibach and co-workers [13,14]. θ-Al_2O_3 ultrathin films grown via this method resulted in ordered alumina films with a thickness of 6 ± 2 Å [8]. A custom-made Ba evaporation source, containing an exothermic Ba ring getter material (SAES Getters Inc.), was used for preparing the BaO/θ-Al_2O_3/NiAl(100) [12]. As described in a previous report [12], this surface was prepared by carrying out Ba deposition and subsequent oxidation in a stepwise fashion. First, a controlled dose of Ba metal was evaporated onto the θ-Al_2O_3/NiAl(100) surface in UHV at 300 K; then O_2(g) ($P_{O_2} = 5 \times 10^{-7}$ Torr) was introduced into the chamber at 300 K. Next, the sample temperature was quickly increased to 800 K in the presence of O_2(g), and the sample was annealed at 800 K for 15 min. These dosing and annealing sequences were repeated for each Ba deposition step (total number of deposition/oxidation steps = 8; total time of Ba deposition = 50 min; 1 ML $< \theta_{Ba}^{total} <$ 2 ML). It was also pointed out in a previous report [12] that for similar model systems, $BaAl_2O_4$ formation also can be observed after high-temperature ($T > 1000$ K) treatments. On the other hand, because the initial sample preparation was done at $T \leqslant 800$ K here, the surface was dominated by BaO species rather than $BaAl_2O_4$. TPD experiments were performed using a differentially pumped QMS by applying −70 V bias voltage on the spectrometer shield to constrain the ionizing electrons to the interior of the QMS shield, preventing any possible electron beam damage on the sample. All of the TPD data presented in this study were obtained by ramping the temperature of the sample at a constant rate of 2 K/s. A tubular pinhole gas doser, positioned in close proximity to the sample (∼2 mm away), was used in the adsorption/desorption (TPD) experiments, which allowed the background pressure in the chamber to stay in the $\sim 10^{-10}$ Torr range during the dosing processes, minimizing background desorption artifacts in the TPD data.

Before the introduction of NO_2 gas to the vacuum chamber, the gas-dosing line and pinhole doser were passivated by flushing with NO_2 gas for an extended period. This passivation procedure was monitored with QMS by following the 46-amu signal with respect to the 30-amu signal for a constant flux of NO_2. The saturation of the 46/30-amu ratio indicated the deactivation of the dosing line surfaces. This procedure was found to be helpful in minimizing the decomposition of NO_2 before admittance to the vacuum chamber. XPS data were acquired using an Al$K\alpha$ X-ray source ($h\nu = 1486.6$ eV) and 50 eV pass energy. The X-ray source was oriented ∼50° with respect to the sample normal.

3. Results and discussion

Fig. 1 illustrates the procedure used for the synthesis of the BaO/θ-Al_2O_3/NiAl(100) model system [11,12]. In this procedure, the NiAl(100) surface (Fig. 1a) was cleaned and used as a substrate to grow the θ-Al_2O_3/NiAl(100) ultrathin film (Fig. 1b) [8,13–17]. Next, the BaO layer was prepared via a step-by-step growth protocol as described in Section 2. In this protocol, Ba metal is dosed on a clean θ-Al_2O_3/NiAl(100) surface at 300 K in UHV, resulting in a well-dispersed Ba surface

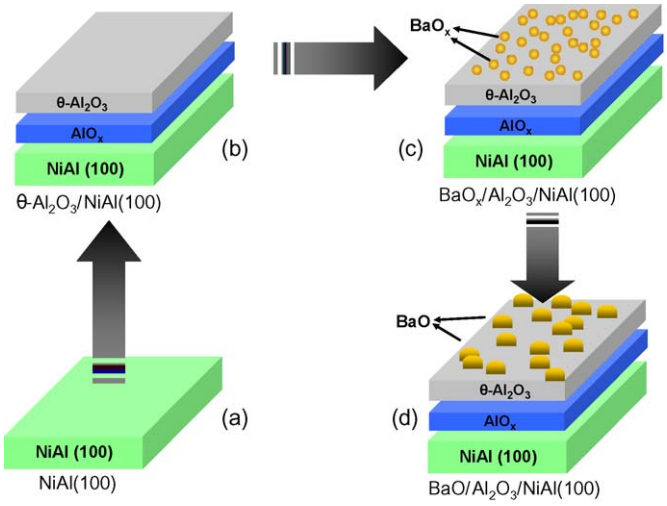

Fig. 1. Preparation protocol that is followed to synthesize BaO/θ-Al_2O_3/NiAl-(100) model system (see text for details). (a) Clean NiAl(100) bimetallic substrate, (b) θ-Al_2O_3 ultrathin film grown on NiAl(100), (c) Ba deposition on θ-Al_2O_3/NiAl(100), (d) BaO/θ-Al_2O_3/NiAl(100) model system obtained after stepwise Ba deposition/oxidation.

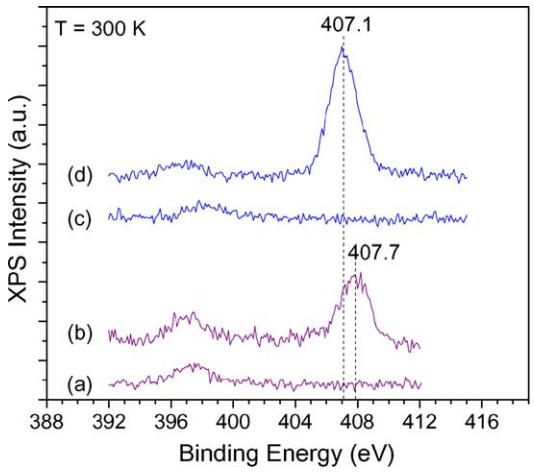

Fig. 2. XPS data for (a) clean θ-Al_2O_3/NiAl(100) surface at 300 K, (b) θ-Al_2O_3/NiAl(100) surface after NO_2 adsorption at 300 K ($P_{NO_2} = 1.5$ Torr, total NO_2 exposure $= 4.5 \times 10^8$ L) and pumping out at 300 K, (c) clean BaO/θ-Al_2O_3/NiAl(100) surface at 300 K, (d) BaO/θ-Al_2O_3/NiAl(100) surface after NO_2 adsorption at 300 K ($P_{NO_2} = 1.5$ Torr, total NO_2 exposure $= 4.5 \times 10^8$ L) and pumping out at 300 K. Spectra were shifted for clarity.

component that strongly interacts with the oxygen-terminated θ-Al_2O_3/NiAl(100) surface (Fig. 1c) [11]. Subsequently, the Ba-dosed surface is annealed in O_2 at 800 K for each Ba deposition step, leading to the formation of fully oxidized 3D BaO clusters (Fig. 1d) [12]. The total BaO coverage at the end of the deposition and oxidation series is within 1 monolayer equivalent (MLE) $< \theta_{Ba} <$ 2 MLE [12]. During oxidation and growth of the 3D BaO clusters, film thickening and a loss in the order of the alumina film structure are also observed [12].

Fig. 2 presents XPS results comparing the N1*s* regions of the XPS data corresponding to θ-Al_2O_3/NiAl(100) and BaO/θ-Al_2O_3/NiAl(100) surfaces before and after NO_2 uptake. In these experiments, after the XP spectrum of the clean surfaces at room temperature were acquired (spectra a and c in Fig. 2), the samples were transported to the elevated pressure cell and saturated with NO_2(g) at 300 K ($P_{NO_2} =$ 1.5 Torr, total NO_2 exposure $= 4.5 \times 10^8$ L, where L $= 1 \times 10^{-6}$ Torr s). After evacuation, the samples were moved back to the main UHV chamber, and XPS data were obtained at 300 K. The XPS data shown in Fig. 2 clearly indicate that saturating θ-Al_2O_3/NiAl(100) (Fig. 2b) and BaO/θ-Al_2O_3/NiAl(100) (Fig. 2d) surfaces with NO_2 at 300 K resulted in the formation of nitrate species, as evident from the N1*s* features at 407.7 and 407.1 eV, respectively [9,18]. In contrast, considering the noticeable dissimilarity in the binding energy values of the nitrate species, various differences in the adsorption sites, adsorption strengths, or surface coordinations of these nitrate species were likely over these two materials (consistent with the TPD results discussed below). XPS experiments were also carried out by dosing lower exposures of NO_2 (0–20 L) on the BaO/θ-Al_2O_3/NiAl(100) surface at 80 K and the thermal evolution of N1*s* species at 80–850 K was monitored (results not shown). The results of these experiments were qualitatively similar to those obtained for the θ-Al_2O_3/NiAl(100) surface [9], where the surface was dominated by nitrate species at $T > 180$ K, whereas at $T < 180$ K, BaO/θ-Al_2O_3/NiAl(100) surfaces were populated with mostly molecular species, such as NO_2 and N_2O_4(NO_2-dimer), with a minor contribution from nitrite species. The results of this XPS experiment indicated that from physisorbed NO_2/N_2O_4 nitrites formed first on both the θ-Al_2O_3/NiAl(100) and BaO/θ-Al_2O_3/NiAl(100) surfaces. As the sample temperature was increased, the nitrites were gradually converted into nitrates; at elevated temperatures, the only ionic NO_x species observed were nitrates. These results are consistent with the previously proposed formation mechanism of the ionic NO_x species—that is, on exposure of BaO/alumina systems to NO_2, first nitrites form, and then these nitrites are converted to nitrates. In situ vibrational spectroscopic studies are currently underway to further examine the NO_x species on this model system at both cryogenic and elevated temperatures. The most significant implication of the XPS results given in Fig. 2 is that, in accordance with previous reports on high-surface area BaO/γ-Al_2O_3 and γ-Al_2O_3 catalysts [2,19,20], nitrate species are formed on NO_2 adsorption on θ-Al_2O_3/NiAl(100) and BaO/θ-Al_2O_3/NiAl(100) surfaces at room temperature. In addition, comparing the intensities of the nitrate signals in the XPS data shown in Fig. 2 emphasizes the significantly higher NO_x uptake by the BaO/θ-Al_2O_3/NiAl(100) model storage system with respect to that of the θ-Al_2O_3/NiAl(100) support.

Fig. 3 presents TPD results for the NO_2/θ-Al_2O_3/NiAl(100) adsorption system for various adsorbate coverages. A comprehensive discussion of these results and the complimentary XPS data can be found elsewhere [9]. TPD (Fig. 3) and XPS [9] experiments reveal that NO_2 [21] adsorbs predominantly in a molecular fashion on the θ-Al_2O_3/NiAl(100) surface at low temperatures by first occupying surface cationic sites in the monolayer, resulting in a perturbed first-order desorption behavior with a temperature desorption maximum at 144 K for $\theta_{NO_2} = 1$ monolayer (ML). After completion of the ML, formation of physisorbed NO_2 multilayers is evident, which leads

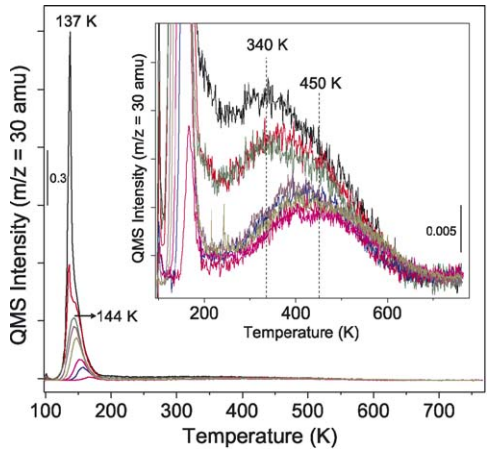

Fig. 3. 30-amu desorption signal in the TPD data for NO_2 adsorption at 80 K on a clean θ-Al_2O_3/NiAl(100) surface. The inset presents a detailed view of the high-temperature region of the TPD curves.

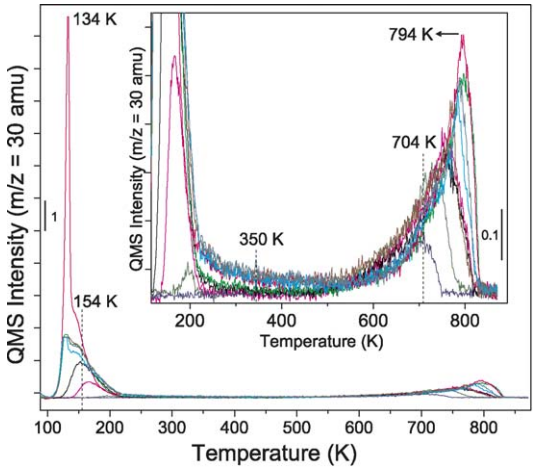

Fig. 4. 30-amu desorption signal in the TPD data for NO_2 adsorption at 80 K on a clean BaO/θ-Al_2O_3/NiAl(100) surface. The inset presents a detailed view of the high-temperature region of the TPD curves.

to desorption maxima at 137 K with typical zero-order desorption characteristics, as is frequently observed for weakly bound multilayer adsorption states. The results of our previous infrared reflection absorption spectroscopy (IRAS) [10] and XPS [9] studies revealed that physisorbed NO_2 multilayers on θ-Al_2O_3/NiAl(100) existed in the form of NO_2 dimers (i.e., N_2O_4). Along with these molecular NO_2 states, a smaller quantity (<0.4 ML) of strongly bound ionic NO_x surface species yielding 30-amu TPD maxima between 350 and 450 K was observed, as shown in the inset of Fig. 3. Although these strongly bound ionic species existed in the form of surface nitrates (NO_3^-) and nitrites (NO_2^-) at 180–300 K, at $T > 300$ K only nitrate species were present on the θ-Al_2O_3/NiAl(100) surface [9]. Previous TPD studies [9] revealed that during the decomposition and desorption of these ionic NO_x species at $T >$ 180 K, O_2 or NO_2 desorption was not observed, and only the 30-amu (NO) channel yielded a detectable desorption signal.

NO_x uptake of the BaO/θ-Al_2O_3/NiAl(100) surface was studied in the TPD experiments by varying the NO_2 exposures at 80 K (Fig. 4). The low-temperature region ($T < 250$ K) of the TPD spectra given in Fig. 4 qualitatively resembles that in Fig. 3, where for lower NO_2 exposures, a single desorption feature grew in intensity with a perturbed first-order desorption behavior. The intensity of this feature eventually saturated with increasing NO_2 exposure, resulting in a desorption maximum at 154 K. After the saturation of the 154 K feature, an additional desorption feature developed with intensity monotonically increasing with increasing NO_2 coverage, without saturation. This second desorption feature showed a zero-order behavior, with a desorption maximum at 134 K for the highest NO_2 coverage given in Fig. 4 [22]. Based on the discussion given above and the consistency between the TPD line shapes and the relative intensities of the 30 and 46-amu signals, as well as the N1*s* signal in the XPS measurements obtained under similar experimental conditions (not shown), we attribute the NO_x desorption from the BaO/θ-Al_2O_3/NiAl(100) surface at $T < 250$ K predominantly to molecular NO_x species, namely an NO_2 monolayer desorbing at 154 K and physisorbed NO_2/N_2O_4 multilayers with desorption maxima around 134 K.

As a quantitative comparison, it should be noted that in Fig. 4, the total integrated NO_x desorption signal at 80–850 K for the highest NO_2 exposure used was about five times that of the saturation of the first chemisorbed NO_2 layer on this surface.

Besides these noticeable resemblances between the low-temperature molecular NO_x desorption signals given in Figs. 3 and 4, significant dissimilarities also exist that should be addressed. Comparing the integrated TPD intensity for the molecular NO_2 species just after saturation of the 144 K desorption feature in Fig. 3 and the 154 K feature in Fig. 4 shows that the integrated TPD intensity of the 154 K feature in Fig. 4 is about a factor of 2.5 greater than the 144 K feature in Fig. 3. This observation suggests that a significantly larger quantity of chemisorbed NO_2, which desorbs reversibly in a molecular fashion during the TPD experiments, can be accommodated in the first adsorption layer on the BaO/θ-Al_2O_3/NiAl(100) surface with respect to that on the Ba-free θ-Al_2O_3/NiAl(100) surface. Multiple factors can be associated with this observation. First, the total surface area of the BaO/θ-Al_2O_3/NiAl(100) surface is presumably greater than the Ba-free θ-Al_2O_3/NiAl(100) surface due to the presence of 3D BaO clusters, as well as to the disordering of the alumina substrate during the BaO growth. Second, the higher affinity of BaO sites toward the NO_x species might allow a more densely packed chemisorbed NO_2 layer on the BaO/θ-Al_2O_3/NiAl(100) surface. This is also in line with the fact that the 154 K feature in Fig. 4 shows a significantly broader FWHM compared with the 144 K feature in Fig. 3, implying a greater variety of adsorption sites for chemisorbed NO_2 on the BaO/θ-Al_2O_3/NiAl(100) system. Due to the large surface coverage of BaO on the alumina thin film, a relatively small portion of the alumina support surface is expected to be exposed to the adsorbate gas. This assumption is also consistent with the relatively lower concentration of the strongly bound ionic NO_x species on the alumina sites of the BaO/θ-Al_2O_3/NiAl(100) surface, as discussed below.

NO_x desorption features that appear at $T > 250$ K in Fig. 4 provide valuable insights regarding the NO_x storage behavior of the BaO/θ-Al_2O_3/NiAl(100) model system. The inset in Fig. 4

presents a detailed view of the high-temperature region of the TPD data. An asymmetric desorption signal is apparent at 250–550 K, coinciding with the desorption temperature of the NO_x species that are desorbing from the θ-Al_2O_3/NiAl(100) surface as a result of the decomposition of nitrate species on the alumina sites (Fig. 3). Thus, we attribute the tailing desorption signal in the inset of Fig. 4 at 250–550 K to the desorption of nitrate species residing on the alumina sites of the BaO/θ-Al_2O_3/NiAl(100) model system. For the highest NO_2 exposure given in Fig. 4, the coverage of these alumina-bound nitrate species reaches about 35% of the molecular NO_2 species that are desorbing at 154 K in Fig. 4 [i.e., the saturation of the first NO_2 chemisorption layer on BaO/θ-Al_2O_3/NiAl(100)]. The lack of any O_2 desorption signal (Fig. 5) at 250–550 K also supports this assignment, because our previous TPD study [9] reported that nitrate desorption from the θ-Al_2O_3/NiAl(100) surface results in only NO(g) evolution, where remaining oxygen atoms either decorate surface defects or diffuse into subsurface region of the θ-Al_2O_3/NiAl(100) system. Apparently, diffusion of oxygen into subsurface creates complications in comparing the model system with a realistic counterpart that lacks such a bimetallic substrate. On the other hand, as we will discuss it in the latter part of this paper, the types of NO_x species stored by the model system have a significant resemblance to the real NO_x storage material. Therefore, despite the additional surface phenomena that can occur on the model system, there is a very good correlation between these two cases, which provides valuable detailed information regarding the NO_x storage process in real NSR systems. The thermal window between 550 and 850 K in Fig. 4 also includes an NO desorption signal originating from the decomposition of nitrate species from the BaO/θ-Al_2O_3/NiAl(100) surface. The inset of Fig. 4 clearly shows that a new desorption feature, due to strongly bound nitrate species, starts to appear with desorption maxima that are shifting to higher temperatures (704–794 K) with increasing NO_2 exposures. Comparing Figs. 3 and 4 readily reveals that such a desorption feature is not associated with the nitrate species adsorbed on the alumina sites, because the TPD data presented in Fig. 3 lacks a similar strong desorption signal at $T > 600$ K. Thus, we attribute the desorption features between 550 and 850 K to strongly bound nitrate species on the BaO domains of the BaO/θ-Al_2O_3/NiAl(100) surface. The TPD spectrum corresponding to the lowest NO_2 exposure used in the series of experiments given in the inset of Fig. 4 suggests that at low NO_2 surface coverage, chemisorbed NO_2 species are almost completely converted to strongly bound nitrates (either on the BaO or Al_2O_3 domains) and diffuse onto the BaO domains, presumably forming $Ba(NO_3)_2$, during the TPD experiment. Lack of a NO_x desorption signal between 250 and 500 K for the lowest NO_2 exposure used in Fig. 4 also indicates that, due to the availability of a large number of strongly binding (and also thermodynamically favorable) BaO sites, nitrates formed on the BaO/θ-Al_2O_3/NiAl(100) surface do not populate alumina domains, but rather diffuse onto the BaO domains during the temperature ramp. However, with increasing NO_2 exposure, BaO domains start to be more densely populated with nitrate species, and the nitrate diffusion on the BaO domains and/or $Ba(NO_3)_2$ formation becomes kinetically hindered during the rapid temperature ramp of the TPD experiment. Therefore, some of the nitrate species start to populate less strongly binding adsorption sites on the alumina surface (250–550 K). Furthermore, due to the increasing nitrate concentration on the BaO/θ-Al_2O_3/NiAl(100) surface, at higher NO_2 exposures, not all of the adsorbed NO_2 species can be converted into nitrates, and some of the adsorbed NO_2 molecules begin to desorb reversibly in a molecular fashion at $T < 250$ K. Therefore, it can be argued that during the TPD experiments for very low NO_2 exposures, formation and surface diffusion of nitrate species are not kinetically limited, and the nature of the NO_x species on the BaO/θ-Al_2O_3/NiAl(100) model system is dictated predominantly by thermodynamics. The opposite is true for higher NO_2 exposures; where, due to blocking of the active catalyst sites by chemisorbed NO_2 or nitrate species, not all of the adsorbed NO_2 molecules can be converted into the thermodynamically stable nitrate species, and a large portion of the adsorbed NO_2 molecules desorb reversibly in a molecular fashion before being converted into nitrates during the rapid temperature ramp in TPD. It also should be mentioned that the relatively lower concentration of nitrates on the alumina sites of the BaO/θ-Al_2O_3/NiAl(100) system (i.e., 250–550 K signal in Fig. 4) is consistent with the high BaO surface coverage, preventing direct exposure of most of the alumina surface sites to the gas-phase adsorbate.

The comparison between Figs. 3 and 4 clearly illustrates the drastic improvement in the NO_x storage capacity of the model catalyst system due to the presence of a BaO-containing catalyst component. The integrated TPD intensity (between 550 and 850 K) corresponding to the strongly bound nitrate species on the BaO/θ-Al_2O_3/NiAl(100) surface, for the highest NO_2 exposure used in Fig. 4, is about 5 times greater than the nitrate desorption signal from the θ-Al_2O_3/NiAl(100) surface (between 250 and 650 K) given in Fig. 3. This is in very good agreement with previous studies on high-surface area catalysts in which the BaO (20 wt%)/γ-Al_2O_3 system was reported to have an order of magnitude higher NO_x storage capacity with respect to the γ-Al_2O_3 support material [2]. From a thermodynamic standpoint, the stability of the stored nitrate species are significantly increased as a result of the presence of baria sites in the model catalyst composition. It is also apparent in Fig. 4 that, due to the kinetically limited nitrate formation on the BaO/θ-Al_2O_3/NiAl(100) surface at high NO_2 exposures, the integrated TPD intensity of the NO_x desorption feature within 704–794 K saturates with increasing NO_2 exposures and eventually settles at a value about 75% of the saturation coverage of the first chemisorbed NO_2 layer (154 K in Fig. 4) on this surface. However, as we show below, the saturation of the nitrate desorption signal at 704–794 K in the inset of Fig. 4 does not imply that the maximum nitrate uptake by the BaO/θ-Al_2O_3/NiAl(100) model catalyst is reached.

This is illustrated in a series of TPD experiments presented in Fig. 5. To use the full NO_x storage potential of the BaO/θ-Al_2O_3/NiAl(100) model system, a given exposure of NO_2 (corresponding to the maximum exposure used for the TPD series in Fig. 4) was dosed on the catalyst surface at 80 K, and the

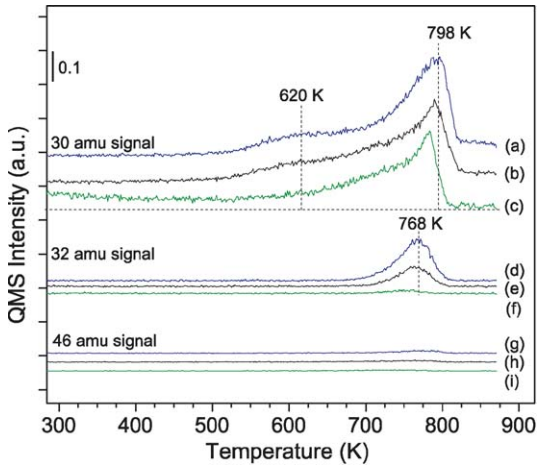

Fig. 5. TPD data obtained after multiple NO_2 dosing/annealing sequences on a clean BaO/θ-Al_2O_3/NiAl(100) surface (see text for details). Spectra c, f, i were obtained after a single NO_2 adsorption at 80 K (without further annealing or additional NO_2 dosing) while spectra b, e, h and a, d, g were obtained after three and six NO_2 dosing (80 K) and annealing (475 K) sequences, respectively. (a–c) 30-amu signal, (d–f) 32-amu signal, (g–i) 46-amu signal.

sample was subsequently annealed at 475 K in UHV for 5 min to convert chemisorbed NO_2 species into nitrates. These low-temperature NO_2 dosing and subsequent annealing steps were repeated various times before the TPD data in Fig. 5 were acquired. The spectra labeled c, f, and i in Fig. 5 correspond to a single NO_2 exposure (i.e., without annealing at 475 K and subsequent NO_2 dosing), whereas spectra b, e, h and a, d, g were obtained by performing NO_2 dosing (80 K) and annealing (475 K) sequences for three and six times before the TPD experiments, respectively. Spectra a, b, and c present the NO desorption (30-amu) signal during these TPD experiments. As discussed above, spectrum c, obtained after a single NO_2 exposure without annealing and subsequent dosing steps, consists of a weak tail at $T < 500$ K, associated with the nitrate species on the alumina sites and a significantly stronger desorption signal at 550–800 K originating from nitrates associated with baria sites of the BaO/θ-Al_2O_3/NiAl(100) surface. The asymmetry of the baria-related nitrate desorption signal in spectrum c (i.e., the presence of multiple desorption features at 620 and 798 K), suggests differences in the adsorption sites, adsorption strengths, and surface coordinations for these nitrate species. Spectrum b, which represents the NO desorption signal in TPD after three dosing and annealing sequences, indicates an increase in the intensities of the shoulder (600–700 K) as well as the high temperature feature at ca. 800 K. Note that spectrum b does not reveal any NO desorption originating from nitrates on the alumina sites (250–500 K), as the model catalyst was annealed at 475 K before the TPD experiment. Spectrum a was obtained after performing six NO_2 dosing (80 K) and annealing (475 K) steps. Comparing spectra a and b suggests that although the intensities of the low-temperature shoulder at 620 K were practically the same, the desorption signal located at 798 K continued to increase with an increasing number of dosing/annealing sequences before the TPD experiment. Quantitative analysis of the TPD desorption signals between 500 and 850 K for spectra a, b, and c reveals that, compared with spectrum c, the NO_x desorption signal increased by 30% in spectrum b and by 50% in spectrum a. These results clearly illustrate that the NO_x uptake of the BaO/θ-Al_2O_3/NiAl(100) model system in the TPD series given in Fig. 4 was kinetically limited at high NO_2 exposures, and an increased NO_x uptake (as high as an additional NO_x storage of 50%) can be achieved by multiple NO_2 loadings and annealing sequences before the TPD experiments.

Further mechanistic details regarding the decomposition of nitrate species on the BaO/θ-Al_2O_3/NiAl(100) model storage system and NO_x release can be extracted from the 32-amu (spectra d, e, and f) and 46-amu (spectra g, h, and i) desorption channels acquired simultaneously with the 30-amu channel given in Fig. 5. The O_2 desorption signal in Fig. 5 suggests that oxygen release by the BaO/θ-Al_2O_3/NiAl(100) surface occurred around 768 K, at a temperature close to the high temperature NO desorption signal at 798 K; although the exact temperature maxima and the TPD line shapes for these two features are somewhat different. Fig. 5 shows that the O_2 desorption signal also exhibited a zero-order desorption behavior, as did the NO desorption signal at 798 K. Furthermore, spectra g, h, and i in Fig. 5 show that that NO_2 desorption signal was essentially zero at 300–850 K (besides an extremely weak feature at ∼780 K in spectrum g).

Based on the foregoing observations, it is apparent that the nitrate decomposition on the baria domains of the BaO/θ-Al_2O_3/NiAl(100) model system can follow different pathways. The O_2 and NO desorption signals at 768 and 798 K suggest that the nitrate species that decomposed at high temperatures (798 K) desorbed via the following pathway:

$$Ba(NO_3)_2 \rightarrow 2NO(g) + \tfrac{3}{2}O_2(g) + BaO. \quad (1)$$

It should be noted that the concentration of these nitrate species does not saturate readily with multiple NO_2 loadings, in contrast to other baria-related nitrate species that desorb at lower temperatures (620 K), with concentration quickly reaching a constant level after the third NO_2 loading/annealing sequence. The desorption mechanism for the low-temperature (620 K) baria-related nitrate species seems to follow a different pathway, because neither O_2 nor NO_2 desorption was observed at $T < 700$ K. One possible decomposition mechanism for these nitrate species could be

$$Ba(NO_3)_2 \rightarrow BaO + 2NO_2^*(ads) + O(ads), \quad (2)$$

$$NO_2^*(ads) \rightarrow NO(g) + O(ads), \quad (3)$$

$$O(ads) \rightarrow O(subsurface), \quad (4)$$

where the nitrate species could dissociate to produce atomic oxygen and a metastable NO_2^* (molecular NO_2 and/or a nitrite) species, which further decompose to yield NO(g) and adsorbed atomic oxygen. Subsequently, adsorbed oxygen atoms can diffuse into the subsurface region and oxidize the Al^0 sites of the NiAl(100) bimetallic substrate (resulting in thickening of the alumina film [9]) or decorate the surface defects of the alumina or BaO domains.

Comparing the NO_x uptake results for the BaO/θ-Al_2O_3/NiAl(100) model system with a realistic high-surface area catalyst reveals very important similarities between these two systems. Fig. 6 presents such a comparison, where the 30-amu

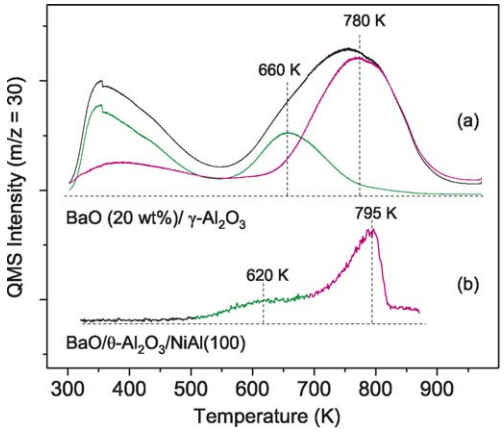

Fig. 6. (a) 30-amu desorption signal in TPD for NO_2 adsorption on a BaO (20 wt%)/γ-Al_2O_3 high surface area material. The 30-amu signal is deconvoluted into two desorption features (see text for details): low temperature (660 K) desorption: NO_2, and high temperature (780 K) desorption: NO. (b) 30-amu desorption signal in TPD that is given in Fig. 5a for a BaO/θ-Al_2O_3/NiAl(100) model system after multiple NO_2 adsorption/annealing sequences. Note that the intensities of the TPD spectra given in (a) are not directly comparable to that in (b) because of the differences in their scales.

signal was monitored in TPD after NO_2 adsorption on a BaO (20 wt%)/γ-Al_2O_3 high-surface area material (Fig. 6a) [19] and the BaO/θ-Al_2O_3/NiAl(100) model system studied here (Fig. 6b). The most important aspect of Fig. 6 is the qualitative agreement between these two systems regarding the thermal window of NO_x release (i.e., 500 K < T < 800 K). Therefore, the BaO/θ-Al_2O_3/NiAl(100) model system seems to be a promising platform for studying molecular-level phenomena that occur on the complex industrial counterpart. The broad desorption feature in Fig. 6a at T < 500 K was attributed to weakly bound molecular NO_x species on the BaO (20 wt%)/γ-Al_2O_3 high-surface area system [19], whereas the asymmetric desorption feature at T > 550 K was assigned to the nitrate species associated with the baria domains. As described in detail in a previous report [19], the NO desorption signal in Fig. 6a can be deconvoluted into two components (low and high temperature ones). The feature with a desorption maximum at 660 K was assigned to the nitrate decomposition originating from surface nitrates on the baria domains of BaO (20 wt%)/γ-Al_2O_3, which decompose to yield NO_2(g) and O_2(g) as follows:

$$Ba(NO_3)_2 \rightarrow BaO + 2NO_2(g) + O(ads), \quad (5)$$

$$O(ads) + O(ads) \rightarrow O_2(g). \quad (6)$$

The other component (high temperature feature in Fig. 6) obtained after the deconvolution of the total 30-amu signal (black curve) was suggested to be [19] due to the decomposition of bulk nitrates, or $Ba(NO_3)_2$, formed in the subsurface region of the BaO domains. These species were found to desorb as in reaction (1) by yielding NO(g) and O_2(g). This previously proposed model [19] regarding the presence of surface and bulk nitrates on the BaO (20 wt%)/γ-Al_2O_3 high-surface area material is in good agreement with our current results on the BaO/θ-Al_2O_3/NiAl(100) model system, where at least two different types of baria-related nitrate decomposition signals were detected in TPD (Figs. 5 and 6) with desorption maxima in good correlation with that of the high-surface area counterpart. Furthermore, the decomposition products appearing at T > 768 K are in the form of NO(g) + O_2(g), in line with the decomposition products of bulk nitrates of the BaO (20 wt%)/γ-Al_2O_3 high-surface area material. Similarly, the 620 K desorption feature for the model system given in Figs. 5 and 6, whose total intensity readily saturates after a certain NO_2 exposure, is consistent with a surface nitrate assignment. It can be argued that although decomposition of surface nitrates can produce NO_2 on both model and high-surface area systems, the fate of the produced NO_2 species differs in these two cases—molecular desorption as in reaction (5) and decomposition as in reactions (2) and (3). Furthermore, a previous study [12] found that peroxide species can also exist on the BaO/θ-Al_2O_3/NiAl(100) model system in the presence of an oxidizing agent such as O_2. Thus, there might be alternative sources of oxygen desorption in addition to that shown in reaction (6), which may include decomposition of BaO_2 species into BaO by releasing oxygen.

The influence of thermal aging on the NO_x uptake of a model NSR catalyst was studied by preparing a BaO/θ-Al_2O_3/NiAl(100) surface as described in Section 2 and then annealing at 1100 K in UHV for 15 min. Our previous results [12] on the thermal behavior of the BaO/θ-Al_2O_3/NiAl(100) surface in UHV suggest that the baria component of the model system is not stable above ∼1000 K. The primary effect of a high-temperature (T > 1000 K) treatment is the decomposition of BaO domains to yield metallic Ba, which desorbs from the surface, leading to a loss of surface barium coverage. In addition to these processes, some other thermally induced surface phenomena, such as interdiffusion of BaO and alumina components of the model catalyst surface to yield $BaAl_2O_4$-like (barium aluminate) domains, are also possible.

Fig. 7 presents the results of TPD experiments performed by exposing a BaO/θ-Al_2O_3/NiAl(100) surface preannealed at 1100 K to various NO_2 exposures. The highest NO_2 exposure used in Fig. 7 was about two times greater than that used in Fig. 4. Comparing the low-temperature region (T < 250 K) of the TPD spectra in Fig. 7 to that in Fig. 4 demonstrates significantly broadened desorption signals corresponding to the molecular NO_2 states in Fig. 7, indicating the presence of additional adsorption sites. Besides the physisorbed NO_2/N_2O_4 multilayer desorption feature at ∼133 K, two extra features at 156 and 180 K, corresponding to additional NO_2 chemisorption states, are visible. At 250–600 K, NO desorption associated with the nitrates on alumina sites of the model system is observed. This is followed by an NO_x desorption signal associated with nitrates on the baria domains, leading to an NO desorption maxima at 730–808 K. Fig. 7 clearly shows that the relative NO_x uptake by the alumina and baria domains of the BaO/θ-Al_2O_3/NiAl(100) surface preannealed at 1100 K was significantly different than a freshly prepared model system (Fig. 4). The integrated TPD intensity corresponding to nitrates on the baria component of the model catalyst surface for the highest NO_2 exposure used in Fig. 7 was only about 30% of the baria-related NO_x signal in Fig. 4. This observation clearly shows that although a significantly higher NO_2 exposure was used in Fig. 7, due to the reduced NO_x storage

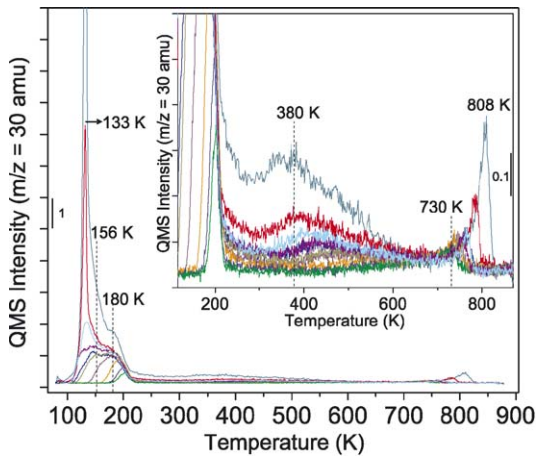

Fig. 7. 30-amu desorption signal in the TPD data for NO_2 adsorption at 80 K on a thermally aged BaO/θ-Al_2O_3/NiAl(100) model system at 1100 K. The inset presents a detailed view of the high-temperature region of the TPD curves.

capacity of the thermally aged model system, a smaller quantity of NO_x was stored by the baria component. In contrast, comparing the integrated TPD intensities associated with nitrate species on the alumina sites of the model surfaces in Figs. 3 [θ-Al_2O_3/NiAl(100)], 4 [fresh BaO/θ-Al_2O_3/NiAl(100)], and 7 [BaO/θ-Al_2O_3/NiAl(100) preannealed at 1100 K] clearly shows that the surface coverage of the nitrates on alumina sites in Fig. 7 was about three times greater than in Fig. 4 and six times greater than in Fig. 3. This observation is consistent with a decrease in the surface coverage of BaO domains after annealing at 1100 K, resulting in uncovering of the alumina sites. Furthermore, an increase in the overall surface area of the model storage system may be responsible for the larger nitrate population associated with the alumina sites in Fig. 7. It is also worth mentioning that in TPD experiments conducted after multiple NO_x loading and release cycles at $T \leqslant 850$ K, very similar NO_x desorption profiles were seen. However, the NO_x uptake of the model system per given dose of NO_2 seemed to decrease very slowly after multiple cycles, similar to the catalytic aging features on extended operation in real systems. In these model systems, the slow storage capacity decrease may originate from the loss of active BaO storage phase (by either desorption or interdiffusion with the thin alumina film).

4. Summary and conclusions

In this work we have investigated the NO_x uptake of various model NO_x storage materials [i.e., θ-Al_2O_3/NiAl(100), BaO/θ-Al_2O_3/NiAl(100) and thermally-aged BaO/θ-Al_2O_3/NiAl(100) at 1100 K] via NO_2 adsorption using XPS and TPD techniques. The primary goal of this contribution was to demonstrate the validity of the proposed model system discussed here in studying the NO_x chemistry on these model NO_x storage materials. In our ongoing efforts, we are concentrating on the details of NO_x uptake and release processes on these model storage systems using a wide array of analytical tools (RAIRS, XPS, ISS, TPD, and scanning probe techniques).

The experimental results of this work can be summarized as follows:

(a) For all of the surfaces listed above, NO_2 adsorption at $T <$ ~200 K led to predominantly molecular NO_x species (NO_2 and N_2O_4) on the catalyst surfaces, whereas by 300 K, these molecular NO_x species either reversibly desorbed or were converted into nitrates.

(b) Nitrate species on the alumina domains of the BaO/θ-Al_2O_3/NiAl(100) model catalyst desorbed at 250–600 K, whereas nitrates residing on the baria domains desorbed at $T > 600$ K, indicating the greater adsorption energy and the improved stability of nitrates in the latter case.

(c) BaO/θ-Al_2O_3/NiAl(100) model catalysts showed significantly enhanced NO_2 adsorption and NO_x storage (nitrate formation) capacity with respect to the θ-Al_2O_3/NiAl(100) support material.

(b) At least two different types of nitrate species were found to exist on the baria domains of the BaO/θ-Al_2O_3/NiAl(100) model NO_x storage material, which decomposed at 620 and 795 K with dissimilar desorption products [NO(g) vs NO(g) + O_2(g)]. Although the intensity of the nitrate signal at 620 K readily saturated with multiple NO_2 loadings before the TPD experiments, the intensity of the 795 K feature continued to grow. These observations are consistent with a previously proposed model in the literature in which NO_x desorption signals at 660 and 780 K were attributed to the presence of surface and bulk nitrates on the baria domains of the BaO (20 wt%)/γ-Al_2O_3 high-surface area catalyst.

(e) Thermal aging of BaO/θ-Al_2O_3/NiAl(100) at 1100 K resulted in a significant reduction of the NO_x uptake by the baria domains of the model catalyst due to Ba evaporation and a corresponding decrease in surface Ba coverage or Ba interdiffusion into the alumina matrix to form $BaAl_2O_4$. In contrast, the weakly bound nitrate population was significantly larger on the alumina-like sites of the thermally aged catalyst than on a fresh BaO/θ-Al_2O_3/NiAl(100) model catalyst or θ-Al_2O_3/NiAl(100) support material. This can be explained by an increased surface area of the alumina sites due to morphological changes.

Acknowledgments

The authors gratefully acknowledge the U.S. Department of Energy (DOE), Office of Basic Energy Sciences, Division of Chemical Sciences for the support of this work. The research described in this paper was performed in the Environmental Molecular Sciences Laboratory, a national scientific user facility sponsored by the DOE Office of Biological and Environmental Research and located at Pacific Northwest National Laboratory (PNNL). PNNL is operated for the DOE by Battelle Memorial Institute under contract DE-AC05-76RL01830. The authors thank Dr. Zdenek Dohnálek for helpful discussions.

References

[1] S. Matsumoto, Cattech. 4 (2000) 102, and references therein.
[2] W.S. Epling, L.E. Campbell, A. Yezerets, N.W. Currier, J.E. Parks II, Catal. Rev. 46 (2) (2004) 163, and references therein.

[3] I. Nova, L. Castoldi, F. Prinetto, V. Dal Santo, L. Lietti, E. Tronconi, P. Forzatti, G. Ghiotti, R. Psaro, S. Recchia, Top. Catal. 30 (1) (2004) 181.
[4] L. Olsson, R.J. Blint, E. Fridell, Ind. Eng. Chem. Res. 44 (2005) 3021.
[5] R.M. Heck, R.J. Farrauto, Catalytic Air Pollution Control: Commercial Technology, Thompson, New York, 1995.
[6] P. Stone, M. Ishii, M. Bowker, Surf. Sci. 537 (2003) 179.
[7] Y. Sakamoto, K. Okumura, Y. Kizaki, S. Matsunaga, N. Takahashi, H. Shinjoh, J. Catal. 238 (2006) 361.
[8] E. Ozensoy, J. Szanyi, C.H.F. Peden, J. Phys. Chem. B 109 (2005) 3431.
[9] E. Ozensoy, C.H.F. Peden, J. Szanyi, J. Phys. Chem. B 109 (2005) 15,977.
[10] E. Ozensoy, C.H.F. Peden, J. Szanyi, J. Phys. Chem. B 110 (2005) 8025.
[11] E. Ozensoy, C.H.F. Peden, J. Szanyi, J. Phys. Chem. B, in press.
[12] E. Ozensoy, C.H.F. Peden, J. Szanyi, J. Phys. Chem. B, in press.
[13] P. Gassmann, R. Franchy, H. Ibach, Surf. Sci. 319 (1994) 95.
[14] P. Gassmann, R. Franchy, H. Ibach, J. Electron. Spectrosc. Relat. Phenom. 64–65 (1993) 315.
[15] N. Fremy, V. Maurice, P. Marcus, J. Am. Ceram. Soc. 86 (2003) 669.
[16] N. Fremy, V. Maurice, P. Marcus, Surf. Interface Anal. 34 (2002) 519.
[17] V. Maurice, N. Fremy, P. Marcus, Surf. Sci. 581 (2005) 88.
[18] Note that the feature at 397 eV is a background artifact originating from the θ-Al_2O_3/NiAl(100) substrate.
[19] J. Szanyi, J.H. Kwak, D.H. Kim, S.D. Burton, C.H.F. Peden, J. Phys. Chem. B 109 (2005) 27.
[20] B. Westerberg, E. Fridell, J. Mol. Catal. A 165 (2001) 249.
[21] As discussed in detail in Ref. [9], it is well known that NO_2 fragments into lower mass components during its ionization in the QMS, and 30 amu (NO) is dominant. Therefore, the relative intensities of the 46- and 30-amu signals as well as the similarity between the line shapes clearly indicate that the 30-amu desorption features observed for $T < 180$ K in this work are predominantly due to the fragmentation of molecular NO_2 in the QMS whereas the 30-amu signal desorbing at $T > 180$ K is attributed to ionic species that thermally decompose to yield gas-phase NO.
[22] For some of the TPD traces given in Fig. 4, intensities of the 134 K features are cut-off, because of the saturation of the QMS multiplier that is operated at a higher sensitivity setting in these TPD measurements.